$ZnAl_2O_4$. Hence, at the beginning of the nucleation the nanocrystallites contain $Zn(Al_{2-x}Cr_x)_2O_4$ characterized with x values close to 1, whereas for higher temperatures Cr^{3+}-doped gahnite nanocrystallites are characterized by small x values that overlap with the previous ones. The model of the nucleation and crystallization processes in the SiO_2–ZnO–Al_2O_3–Cr_2O_3 system has been summarized in Figure 10.

We believe that these new results will have large consequences on the interpretation of the spectroscopic properties of Cr^{3+}-doped materials because we now have the possibility of accurately connecting our characterized samples with the emission spectra of both strong and weak crystal field sites.

Conclusion

Xerogels of the SiO_2–Al_2O_3–ZnO system doped by Cr_2O_3 have been synthetized by varying the proportions of the different components. Under heat treatments between 50 and 1000 °C it has been demonstrated that chromium evolves from Cr^{3+}-doped aqueous media at low temperature to Cr^{6+} ions up to 800 °C and then again to Cr^{3+}-doped both in glassy and crystalline phases. X-ray diffraction, small-angle X-ray scattering, and transmission electron microscopy support the conclusion that gahnite-like structure nanocrystallites grow. The average sizes measured in the final glass–ceramic varied from 5 to 21 nm. Such xerogel does not contain pores greater than 1 nm which are bounded by surfaces with fractal dimension $D_s = 2.5$ in nonnucleated samples, whereas nucleated samples cannot be easily explained with a fractal model. The lattice constant changes from $a_0 = 8.30$ Å (close to $ZnCr_2O_4$) at 800 °C to $a_0 = 8.0812$ Å (close to $ZnAl_2O_4$) at 1000 °C. The nucleation appears to form stoichiometric gahnite with the general formula $Zn(Cr_xAl_{1-x})_2O_4$ ($1 > x > 0$). After saturation of ZnO in crystallites, the two other constituents SiO_2 and Al_2O_3 of the xerogel form a mullite glass. The Cr^{3+} fluorescence allows us to detect glassy and crystalline phases and especially the different local environments which evolve during the crystallization mechanism. A direct relation has been made between octahedral crystallographic sites and the presence of lines and emission bands in nanocrystallites. This has important consequences for our understanding of the optical properties of Cr^{3+}-doped gahnite and, also, in a general way, on the properties of luminescent materials owing to well-characterized xerogel samples.

Acknowledgment. This work is supported by Groupement de Recherche (GDR) Verre of CNRS.

Registry No. Al_2O_3, 1344-28-1; ZnO, 1314-13-2; Cr_2O_3, 1308-38-9; gahnite, 1302-75-6.

Effects of Substitution Chemistry in the $KTiOPO_4$ Structure Field

Mark L. F. Phillips,*,† William T. A. Harrison,‡ Galen D. Stucky,‡ Eugene M. McCarron III,§ Joseph C. Calabrese,§ and Thurman E. Gier§

Sandia National Laboratories, Albuquerque, New Mexico 87185; Department of Chemistry, University of California, Santa Barbara, California 93106; and Central Research and Development Department, E. I. du Pont de Nemours, Wilmington, Delaware 19880

Received August 12, 1991

Potassium titanyl phosphate ($KTiOPO_4$, or KTP) is an important nonlinear optical medium whose structure permits a moderate degree of cation mobility. This feature is exploited in the syntheses of $Na_{0.95}K_{0.05}TiOPO_4$ (NaTP), $Ag_{0.85}K_{0.15}TiOPO_4$ (AgTP), and $Na_{0.87}K_{0.13}TiOAsO_4$ (NaTA) from single crystals of KTP and $KTiOAsO_4$ (KTA) through ion exchange at low temperatures, as these compositions do not crystallize in the KTP structure type when prepared from their constituent oxides at high temperatures. All three compounds are orthorhombic, space group $Pna2_1$, with $Z = 8$. For NaTP, $a = 12.611$ (2) Å, $b = 6.2810$ (9) Å, $c = 10.595$ (2) Å; for AgTP, $a = 12.534$ (2) Å, $b = 6.2939$ (9) Å, $c = 10.524$ (1) Å; for NaTA, $a = 12.8884$ (9) Å, $b = 6.4095$ (3) Å, $c = 10.7393$ (6) Å. Crystals of α-$NaTiOPO_4$, the high-temperature polymorph of NaTP, were prepared hydrothermally. This phase crystallizes in the titanite ($CaTiOSiO_4$) structure and is monoclinic, space group $P2_1/c$, with $a = 6.566$ (1) Å, $b = 8.483$ (1) Å, $c = 7.140$ (1) Å, $\beta = 115.25°$, and $Z = 4$. Ti–O coordination distances in the new KTP isostructures do not deviate significantly from those in KTP or KTA. Second harmonic generation intensities measured at 532 nm show that optical nonlinearity in NaTP and AgTP is significantly attenuated from that in KTP and NaTA. These results are accounted for by (1) differences in interactions between K, Na, Ag, and the titanyl oxygen atoms, which influence the mixing of a delocalized excited state into the ground-state bonding and nonbonding framework orbitals, and (2) a decrease in bandgap due to the increased basicity of the oxygen atoms in the arsenate derivatives.

1. Introduction

Potassium titanyl phosphate ($KTiOPO_4$, or KTP) has enjoyed considerable success as a nonlinear optical medium for second harmonic generation (SHG) at 1064 nm due to the high-power conversion efficiencies, high damage threshold, large angular acceptance,[1] and the low sensitivity of its phase matching condition to temperature.[2] Both sum-frequency generation (SFG)[3] and optical parametric

* Author to whom correspondence should be addressed.
† Sandia National Laboratories.
‡ University of California.
§ E. I. du Pont de Nemours.

(1) Fan, T. Y.; Huang, C. E.; Hu, B. Q.; Eckhardt, R. C.; Fan, Y. X.; Byer, R. L.; Feigelson, R. S. *Appl. Opt.* **1987**, *26*, 2391.
(2) Zumsteg, F. C.; Bierlein, J. D.; Gier, T. E. *J. Appl. Phys.* **1976**, *47*, 4980.

0897-4756/92/2804-0222$03.00/0

oscillation (OPO)[4] have been demonstrated in KTP, as has the fabrication of bulk and waveguide electrooptic (EO) modulators.[5] The arsenic-substituted derivative $KTiOAsO_4$ (KTA) possesses similar NLO/EO properties but is superior to KTP for SHG and electrooptic modulation at 1.064 μm.[6]

1.1. KTP Structure. KTP crystallizes in the orthorhombic space group $Pna2_1$, with all atoms on general positions and two formula units per asymmetric unit. The structure consists of helical chains of TiO_6 octahedra parallel to [011] and [0$\bar{1}$1], which are linked by phosphate tetrahedra to form a framework containing one-dimensional channels in which the potassium atoms are located.[7] The open nature of this framework allows these cations to readily diffuse parallel to [001].[8] This is seen in the magnitude and anisotropy of KTP's ionic conductivity[9] and is used to advantage in waveguide manufacture. Channel waveguides can be fabricated on z-cut KTP substrates at low temperatures by exchanging Rb^+, Tl^+, or Cs^+ ions into the surface from nitrate melts; ions are kept from diffusing out of the waveguide by low mobility perpendicular to [001].[10]

In both KTP and KTA,[11] TiO_6 units link in a trans configuration for one of the two structurally independent titanium atoms and cis for the other titanium atom. For each titanium atom there is a short (<1.75 Å) "titanyl" Ti–O bond trans to a long (>2.10 Å) Ti–O bond. This long bond is to a titanyl oxygen atom in the trans titanyl linkage and to a phosphate oxygen atom in the cis titanyl linkage. We can thus view the TiO_6 groups as distorted octahedra in which the Ti atoms are shifted off-center in the direction of the short bond. Similarly distorted octahedral geometries exist in other ferroelectric structure types such as the ilmenite ($LiNbO_3$), perovskite ($BaTiO_3$), and tungsten bronze ($Sr_{1-x}Ba_xNb_2O_6$) families. Understanding the role of this structural feature in determining NLO/EO response is a goal of several theories seeking to define structure/property relationships in these materials.[12,13]

1.2. KTP Theory. In introducing KTP as a nonlinear optical material, Zumsteg et al.[2] reported on the results of their use of Levine's bond charge model[14] to calculate the microscopic susceptibilities in the $K_{1-x}Rb_xTiOPO_4$ system and concluded that the short Ti–O bond lengths in the TiO_6 groups are the principal contributors to the SHG tensor d_{ijk}. Neither the (K,Rb–O) nor the (P–O) bonds are expected to contribute significantly to the total susceptibility. The results of Hansen et al. also define the short Ti=O "titanyl" bond as being responsible for the large nonlinear optical coefficients in KTP.[15] Furthermore, Hansen et al. describe the long Ti–O bonds trans to the titanyl bonds as being unimportant in defining the NLO coefficients. Again, this approach is simplified by neglecting K–O and P–O contributions. Both of these treatments give calculated values of the second harmonic coefficients (Δ_{ijk}) which are substantially less than those observed experimentally. One potential difficulty with calculations of this type is the uncertainty in the dependence of the microscopic susceptibility β_{ijk} upon bond length, which Levine suggests may be quite large. A second problem may lie in the assumption that only β_{ijk} components parallel to bond axes need be considered and that perpendicular components may be neglected. Bergman and Crane have shown this assumption to be invalid for certain systems and that the perpendicular contribution $\beta_\perp$ can even exceed $\beta_\parallel$.[16] A third concern is the possibility that either the ground state or the excited state which is mixed into the ground state upon perturbation is delocalized so that the localized point dipole model no longer applies.

Chen's anionic group model also assigns the distortion of the Ti coordination sphere as the major contributor to d_{ijk} in KTP.[13] In this more extended treatment the electronic hyperpolarizability is defined within an anionic cluster, which in KTP would be the TiO_6^{8-} groups, by the degree of mixing between molecular orbitals with differing distributions of electron density. In KTP the relevant states are the bonding Ti–O orbitals, the nonbonding lone-pair orbitals on the framework oxygen atoms, and one or more antibonding orbitals at some higher energy (not necessarily the LUMO), which are predominantly titanium atom in character and are responsible for ligand-to-metal charge-transfer excited states. Mixing charge-transfer character into the ground states induces anharmonicity into the electron potentials, which results in nonzero β_{ijk} values for each of the TiO_6 groups. The mixing coefficients depend on the degree of distortion, a measure of which is the difference between short and long Ti–O distances.[17] As was the case in the bond charge schemes, neither the K^+ ion nor the phosphate groups are expected to contribute significantly to KTPs optical nonlinearity.

1.3. Why Cation Exchange? The extent to which chemical composition defines nonlinearity in metal oxides is not immediately apparent from the preceding models, other than the dependence of nonlinearity on the presence of highly polarizable bonds or groups. The $ABOXO_4$ composition itself influences structure, with six-coordinate B atoms and four-coordinate X atoms favoring corner-shared tetrahedral-octahedral linkages, but does not guarantee crystallization in the KTP structure type. Without constraints on composition, we can conceive of replacing for B or X any combination of those atoms which can adopt the same coordination numbers as those of the elements being replaced, as long as charges are balanced in the resulting structure. In $KTiOPO_4$ the framework atoms Ti and P can be replaced in a controlled fashion with other transition or main-group metals or other group V elements, respectively. This feature allows us to determine to what extent the atoms in these positions control structural phase and nonlinear polarizability and the precise coordination environment the framework atoms

(3) (a) Baumert, J. C.; Schellenberg, F. M.; Lenth, W.; Risk, W. P.; Bjorklund, G. C. *Appl. Phys. Lett.* **1987**, *51*, 2192. (b) Risk, W. P.; Baumert, J. C.; Bjorklund, G. C.; Schellenberg, F. M.; Lenth, W. *Appl. Phys. Lett.* **1988**, *52*, 85.
(4) Vanherzeele, H.; Bierlein, J. D.; Zumsteg, F. C. *Appl. Opt.* **1988**, *27*, 3314.
(5) Bierlein, J. D.; Ferretti, A.; Brixner, L.; Hsu, Y. *Appl. Phys. Lett.* **1987**, *50*, 1216.
(6) Bierlein, J. D.; Vanherzeele, H.; Ballman, A. A. *Appl. Phys. Lett.* **1989**, *54*, 783.
(7) Tordjman, I.; Masse, R.; Guitel, J. C. *Z. Kristallogr.* **1974**, *139*, 103.
(8) Bierlein, J. D.; Arweiler, C. B. *Appl. Phys. Lett.* **1986**, *49*, 917.
(9) Morris, P. A.; Crawford, M. K.; Ferretti, A.; French, R. H.; Roelofs, M. G.; Bierlein, J. D.; Brown, J. B.; Loiacono, G. M.; Gashurov, G. *Optical Materials: Processing and Science*; Poker, D. B., Ortiz, C., Eds.; Materials Research Society: Pittsburgh, 1989; Vol. 152, p 95.
(10) Bierlein, J. D.; Ferretti, A.; Brixner, L.; Hsu, Y. *Appl. Phys. Lett.* **1987**, *50*, 1216.
(11) El Brahimi, M.; Durand, J. *Rev. Chim. Mineral.* **1986**, *23*, 146.
(12) Levine, B. F. *Phys. Rev. B* **1976**, *13*, 5102.
(13) Chen, C.-T. *Annu. Rev. Mater. Sci.* **1986**, *16*, 203.
(14) Levine, B. F. *Phys. Rev. B* **1973**, *7*, 2600.
(15) Hansen, N. K.; Protas, J.; Marnier, G. *C. R. Acad. Sci. Paris, Ser. II*, **1988**, *307*, 475.
(16) Bergman, J. G.; Crane, G. R. *J. Chem. Phys.* **1974**, *60*, 2470.
(17) Phillips, M. L. F.; Harrison, W. T. A.; Gier, T. E.; Stucky, G. D.; Kulkarni, G. V.; Burdett, J. K. *Inorg. Chem.* **1990**, *29*, 2158.

Table I. Crystallographic Data

	α-$NaTiOPO_4$	β-$NaTiOPO_4$	$AgTiOPO_4$	$NaTiOAsO_4$
formula	$NaTiPO_5$	$Na_{0.95}K_{0.05}TiPO_5$	$Ag_{0.85}K_{0.15}TiPO_5$	$Na_{0.87}K_{0.13}TiAsO_5$
formula wt	181.86	182.70	256.48	225.81
a, Å	6.556 (1)	12.611 (2)	12.534 (2)	12.8884 (9)
b, Å	8.483 *1(	6.2810 (9)	6.2939 (9)	6.4095 (3)
c, Å	7.140 (1)	10.595 (2)	10.524 (1)	10.7393 (6)
β, deg	115.25 (1)	90	90	90
vol, Å^3	359.7	839.23	830.21	887.15
approx cryst dimens, mm	0.4 × 0.3 × 0.37	0.2 × 0.15 × 0.3	0.3 × 0.25 × 0.1	0.5 × 0.3 × 0.2
no. of reflns centered	19	20	12	21
octants collected	$+h,+k,+l$; $+h,-k,+l$; $-h,-h,+k,+l$; $-h,-k,+l$	$+h,+k,+l$	$+h,\pm k,\pm l$	$+h,+k,+l$; $-h,-k,-l$
no. of reflns collected	2023	1782	6263	3759
no. reflcns obsd	860	1431	4594	3030
merging R factor, %	2.34	N/A	2	2.74
ρ_{calc}, g/cm^3	3.36	2.94	4.13	3.38
μ, cm^{-1}	56.02	26.25	64.3	93.07
transmission coeff				
min	0.25	0.5324	0.2805	0.0489
max	0.38	0.7588	0.4939	0.3222
secondary extinction parameter refined?	yes	yes	yes	no
$R(F_o)$	0.033	0.0539	0.0503	0.0622
$R_w(F_o)$, %	0.043	0.0541	0.0506	0.0639

will have in the resulting structure.

This is not necessarily true in the case of cation exchange. In the KTP structure, cations (the A atoms) are not close-packed but are loosely associated with the framework, as evidenced by the facility with which they can be exchanged for isovalent ions in, for example, waveguide manufacture. Therefore, for a given set of framework atoms, cation substitution, exchange, or inclusion should influence the local coordination environment at the octahedral metal atom site (i.e., metal–oxygen distances) minimally or not at all. In this way the cation–framework interaction is analogous to the host–guest relationship characteristic of more traditional zeolitic materials. This structural control will allow us to determine uniquely the role of the cation in determining framework polarizability.

Nearly all $MTiOPO_4$ and $MTiOAsO_4$ compounds reported to date which can be synthesized directly, rather than by ion exchange, yield SHG intensities which are very similar to KTPs.[18] However, it has been shown that two KTP isostructures prepared by ion exchange, β-$NaTiOPO_4$[19] and β-$AgTiOPO_4$, have SHG intensities which are 1 and 3 orders of magnitude lower, respectively, than KTP's.[20,21] Neither of these "anomalous" compounds can be prepared using the high-temperature methods characteristic of conventional KTP synthesis. Crystallographic results indicated that the Ti–O distances in these compounds remain nearly identical to those in KTP, and it was induced that the cations must strongly influence the observed SHG intensities, though since cation–oxygen bond polarizabilities are predicted to be very slight, the cations presumably alter the electronic structure of the framework rather than contribute directly to the bulk susceptibility $\chi^{(2)}_{ijk}$. In this work we use the ability of KTP and KTA to exchange cations to synthesize compounds unavailable through direct methods and determine the influence this exchange has on the structure and optical properties of the resulting material. The limits of exchange are compared with the extent to which Na and Ag can be substituted into the KTP structure using direct, high-temperature methods. Trends relating the cation-framework bonding and SHG intensities will be discussed in the context of improving on structure/property relationships for this class of compounds. Firstly, though, the synthesis and structural characterization of the centrosymmetric phase α-$NaTiOPO_4$ are described, and its framework structure is compared with that of KTP.

2. Sodium Titanyl Phosphate (α- and β-$NaTiOPO_4$)

The polymorph of $NaTiOPO_4$ isomorphous with KTP, β-$NaTiOPO_4$, or "NaTP" cannot be synthesized directly from stoichiometric quantities of the oxides and therefore lies outside the high-temperature KTP phase space. The polymorph which results from combining the oxides in one-to-one correspondence at high temperature, α-$NaTiOPO_4$, is centrosymmetric and structurally related to the naturally occurring mineral $CaTiOSiO_4$ (titanite, or sphene). Another high-temperature polymorph which will be referred to here as γ-$NaTiOPO_4$ can be precipitated from a Na_2O–P_2O_5 melt containing at least 20 wt % TiO_2.[22] Additional phases which can exist in equilibrium with Na_2O–TiO_2–P_2O_5 melts include $NaTi_2(PO_4)_3$, α-$NaTiOPO_4$, and $Na_4TiO(PO_4)_2$,[23] depending on the temperature and Na/P ratio of the flux.

2.1. α-$NaTiOPO_4$. 2.1.1. Experimental Part. A mixture of TiO_2 (1 mmol), $NaH_2PO_4 \cdot H_2O$ (3 mmol), $Na_2HPO_4 \cdot 7H_2O$ (1 mmol), and 0.30 mL of H_2O were sealed in a $^1/_4$ in. × 3 in. Au tube, which was placed in a pressure vessel. The vessel was pressurized to 3000 bar and heated to 850 °C for 6 h, cooled to 500 °C over 70 h (−5 °C/h), and quenched to room temperature. These conditions resulted in an essentially 100% yield of small crystals of α-$NaTiOPO_4$, from which a suitable single crystal was selected for data collection. The crystal was indexed on an Enraf-Nonius CAD4 single-crystal X-ray diffractometer (graphite monochromated Mo Kα radiation, λ = 0.71069 Å) and found to have a monoclinic unit cell with parameters a = 6.566 (1) Å, b = 8.483 (1) Å, c = 7.140 (1) Å, and β = 115.25 (1)° (see Table I). The cell parameters were

(18) Stucky, G. D.; Phillips, M. L. F.; Gier, T. E. *Chem. Mater.* **1989**, *1*, 492.

(19) The polymorph α-$NaTiOPO_4$ is obtained through high-temperature synthesis and does not crystallize in the KTP structure. See section 2.

(20) Phillips, M. L. F.; Harrison, W. T. A.; Gier, T. E.; Stucky, G. D. *Proc. SPIE—Int. Soc. Opt. Eng.* **1989**, *1104*, 225.

(21) Phillips, M. L. F.; Gier, T. E.; Eddy, M. M.; Keder, N. L.; Stucky, G. D.; Bierlein, J. D. *Solid State Ionics* **1989**, *32/33*, 147.

(22) Nagornyi, P. G.; Kapshuk, A. A.; Stus', N. V.; Slobodyanik, N. S. *Kristallografiya* **1990**, *35*, 634.

(23) Bamberger, C. E.; Begun, G. M.; Cavin, O. B. *J. Solid State Chem.* **1988**, *73*, 317–324.

Table II

(a) Final Atomic Positions and Thermal Parameters for α-$NaTiOPO_4$

atom	x/a	y/b	z/c	B(iso)
Ti(1)	0.74835 (6)	0.25882 (4)	0.52256 (6)	0.3 (1)
P(1)	0.75035 (8)	0.93119 (7)	0.75091 (8)	0.3 (1)
Na(1)	0.2507 (2)	0.4172 (1)	0.2247 (2)	1.6 (1)
O(1)	0.7470 (2)	0.3213 (2)	0.7466 (2)	0.5 (1)
O(2)	0.5704 (2)	0.8201 (2)	0.6007 (2)	0.5 (1)
O(3)	0.9358 (2)	0.8236 (2)	0.9029 (2)	0.5 (1)
O(4)	0.8426 (2)	1.0359 (2)	0.6282 (2)	0.4 (1)
O(5)	0.6531 (2)	1.0332 (2)	0.8717 (2)	0.5 (1)

(b) Bond Distances and Angles in α-$NaTiOPO_4$[a]

Distances, Å

Ti(1)–O(1)a	2.080 (2)	P(1)–O(2)	1.534 (2)
Ti(1)–O(1)	1.689 (2)	P(1)–O(3)	1.539 (2)
Ti(1)–O(2)b	2.008 (2)	P(1)–O(4)	1.541 (2)
Ti(1)–O(3)c	1.986 (2)	P(1)–O(5)	1.539 (2)
To(1)–O(4)d	2.032 (1)	Na(1)–O(1)b	2.227 (2)
Ti(1)–O(5)e	2.023 (1)	Na(1)–O(2)b	2.395 (2)
		Na(1)–O(3)b	2.356 (2)

Angles, deg

O(1)–Ti(1)–O(1)a	179.1 (2)	O(3)–P(1)–O(4)	111.00 (8)
O(1)a–Ti(1)–O(2)b	83.87 (6)	O(3)–P(1)–O(5)	109.33 (9)
O(1)–Ti(2)–O(2)b	95.40 (7)	O(4)–P(1)–O(5)	110.6 (1)
O(1)a–Ti(1)–O(3)c	85.77 (6)	O(1)b–Na(1)–O(2)b	143.77 (7)
O(1)–Ti(1)–O(3)c	94.95 (7)	O(1)b–Na(1)–O(3)b	151.78 (7)
O(1)a–Ti(1)–O(4)d	85.71 (6)	O(2)b–Na(1)–O(3)b	62.05 (6)
O(1)–Ti(1)–O(4)d	93.68 (7)	Ti(1)–O(1)–Ti(1)f	142.6 (1)
O(1)a–Ti(1)–O(5)e	84.56 (6)	Ti(1)b–O(2)–P(1)	149.2 (1)
O(1)–Ti(1)–O(5)e	96.05 (7)	Ti(1)g–O(3)–P(1)	140.8 (1)
O(2)b–Ti(1)–O(3)c	169.64 (7)	Ti(1)h–O(4)–P(1)	128.0 (1)
O(2)b–Ti(1)–O(4)d	87.01 (6)	Ti(1)i–O(5)–P(1)	132.9 (1)
O(2)b–Ti(1)–O(5)e	91.70 (6)	Ti(1)f–O(1)–Na(1)b	103.96 (7)
O(3)c–Ti(1)–O(4)d	92.30 (6)	Ti(1)–O(1)–Na(1)b	113.40 (9)
O(3)c–Ti(1)–O(5)e	87.23 (6)	Ti(1)b–O(2)–Na(1)b	97.82 (6)
O(4)d–Ti(1)–O(5)e	170.26 (6)	Ti(1)g–O(3)–Na(1)b	100.08 (7)
O(2)–P(1)–O(3)	105.7 (1)	P(1)–O(2)–Na(1)b	95.28 (8)
O(2)–P(1)–O(4)	109.2 (1)	P(1)–O(3)–Na(1)b	96.73 (8)
O(2)–P(1)–O(5)	110.91 (8)		

[a] Symmetry operation codes: a, x, $^1/_2 - y$, $z - ^1/_2$; b, $1 - x$, $1 - y$, $1 - z$; c, $2 - x$, $y - ^1/_2$, $^3/_2 - z$; d, x, $y - 1$, z; e, x, $^3/_2 - y$, $z - ^1/_2$; f, x, $^1/_2 - y$, $z + ^1/_2$; g, $2 - x$, $y + ^1/_2$, $^3/_2 - z$; h, x, $y + 1$, z; i, x, $^3/_2 - y$, $z + ^1/_2$.

determined from 19 reflections. Intensity data were collected using the ω scan method, with scan widths from 1.30° to 2.00° and scan speeds from 1.5 to 5.0°/min. Measurements were made from 4.8 to 58.0° 2θ. There was no evidence of radiation damage to the crystal during data collection. The data were corrected for Lorentz and polarization effects, and an azimuthal absorption correction was applied.

The structure was solved using an automated Patterson solution method (PHASE).[24] The model was refined in space group $P21/c$ (No. 14) with full matrix least-squares analysis to $R = 0.033$ and $R_w = 0.043$.[25] The final esd of an observation of unit weight is 2.34. The largest final difference–Fourier residual was 0.69 e/Å^3 near the phosphorus atom.

Table IIa lists the final positional and anisotropic thermal parameters for α-$NaTiOPO_4$. The coordinates are labeled for compatibility and comparison with the isomorphous structure $CaTiOSiO_4$ (sphene),[26] with the exception of our use of the standard space group. Bond distances are given in Table IIb.

Figure 1 depicts the α-$NaTiOPO_4$ unit cell. As seen in this figure and as described in Table IIb, the tetrahedral coordination of phosphorus is fairly regular, while the octahedral coordination of titanium displays the distorted titanyl-type (O═Ti—O_5) arrangement found in $KTiOPO_4$ itself. In fact, the 1.689-Å Ti(1)–O(1) bond is shorter than either of the titanyl bonds in KTP (1.718 and 1.738 Å). However, unlike the cis–trans arrangement of the titanyl chains in $KTiOPO_4$, the titanyl chains of α-$NaTiOPO_4$ are linked in an all-trans configuration (Figure 2). This difference in the connectivity of the Ti–P–O framework can be seen as a consequence of the large difference in the ionic radii of Na^+ and K^+. In $KTiOPO_4$, the framework provides both 8- and 9-fold coordination sites for the larger potassium ion, while in α-$NaTiOPO_4$, the relative placement of the TiO_6 titanyl chains and the PO_4 groups results in a 6-fold, trigonal-pyramidal coordination for the smaller sodium ion. The greater calculated density of α-$NaTiOPO_4$ (3.36 versus 2.94 g/cm^3 for β-$NaTiOPO_4$) also suggests a more efficient packing arrangement in this phase. The

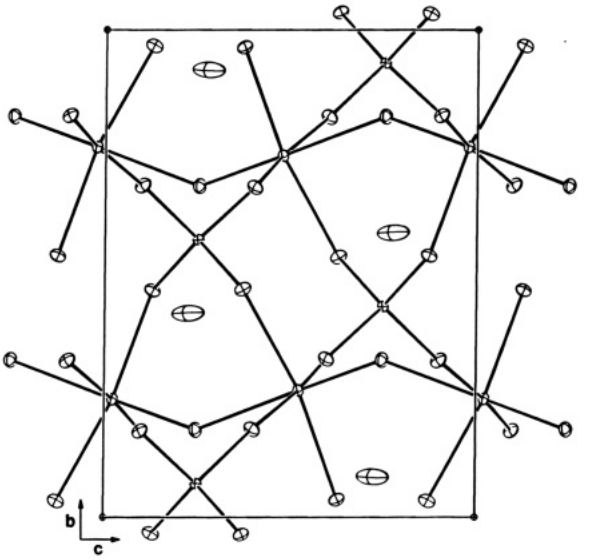

Figure 1. View of the α-$NaTiOPO_4$ unit cell along [100]. The all-trans titanyl chains run parallel to the c axis.

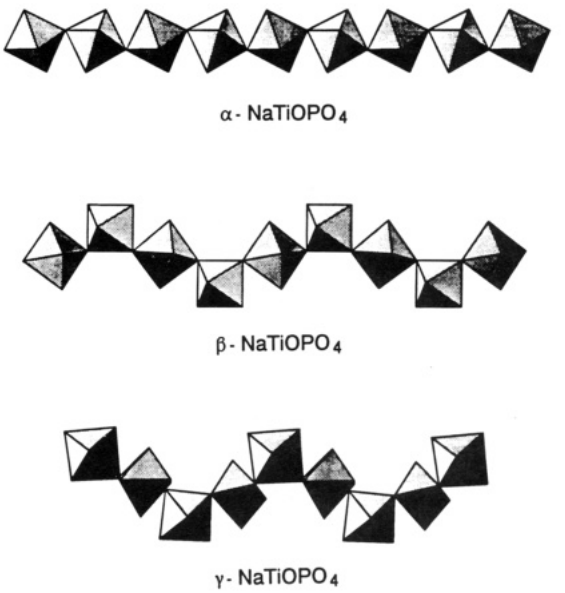

Figure 2. Comparison of the titanyl chains in the various $NaTiOPO_4$ polymorphs: top, all-trans α; center, cis-trans β; bottom, all-cis γ.

(24) Crystallographic calculations were performed on a DEC/CRAY computer network using a system of programs developed by J. C. Calabrese. This package incorporates the ORTEP plot program (C. K. Johnson, 1971).

(25) Complex, neutral atom scattering factors were obtained from: *International Tables for X-ray Crystallography*; International Union for Crystallography: Birmingham, 1974; Vol. IV, Table 2A.

(26) Taylor, M.; Brown, G. E. *Am. Mineral.* **1976**, 435.

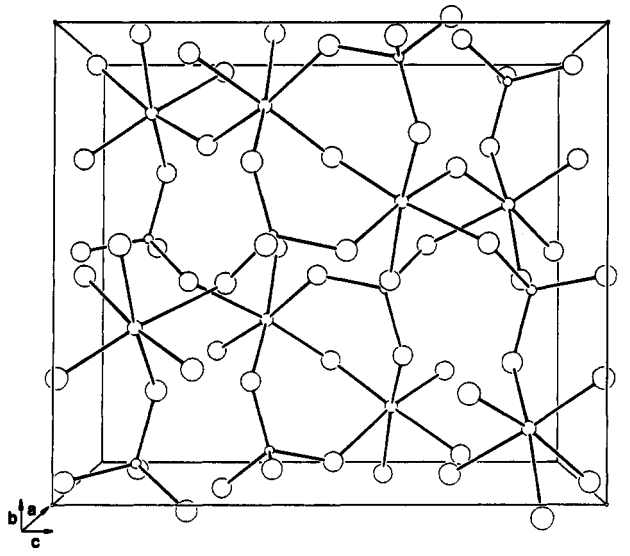

Figure 3. Structure of γ-$NaTiOPO_4$, viewed along [100]. The sodium atoms have been omitted for clarity.

α-$NaTiOPO_4$ structure is thus thermodynamically favored at high concentrations of sodium in $Na_{1-x}K_xTiOPO_4$.

The γ-$NaTiOPO_4$ structure is reported to be orthorhombic, space group $P2_22_12_1$, with a = 8.755 (1) Å, b = 9.124 (1) Å, and c = 10.518 (2) Å.[22] This is a noncentrosymmetric space group, and $\chi^{(2)}$ effects are therefore allowed, though no NLO data have been reported for this phase to date. The structure is similar to both α- and β-$NaTiOPO_4$ in that it consists of TiO_6 chains cross-linked by orthophosphate groups (Figure 3), except that the chain linkages are all cis with respect to the central Ti atoms (Figure 2).

2.2. β-$NaTiOPO_4$ (NaTP). The preceding results indicate that no KTP isostructure with the formula $NaTiOPO_4$ is available using conventional high-temperature methods. This suggests that this structure is unstable under the conditions required for direct synthesis. However, ion exchange affords the possibility that this material can be prepared via a low-temperature route. The focus of this investigation is to learn whether ion exchange can yield KTP-type structures unavailable through direct synthesis and to determine the influence of sodium exchange on the structure and optical properties of the resulting compound.

2.2.1. Synthesis. A melt prepared by heating 1.60 g of TiO_2, 8.64 g of KH_2PO_4, and 1.44 g of $K_2HPO_4{\cdot}3H_2O$ (Fisher) to 1000 °C in a 30-mL Pt crucible was cooled from 950 to 910 °C at the rate of 1 °C/h. The supernatant flux was then poured off and discarded, and the insoluble crystals were allowed to cool in the furnace. The cooled flux was dissolved in hot water, and the crystals were recovered by filtration; 0.93 g of $KTiOPO_4$ was obtained, with crystal sizes ranging from fine powder to 1-mm-diameter pieces. Many crystals were of good quality, lacking either twins or flux inclusions.

KTP crystals (0.089 g) with approximate diameters between 0.2 and 0.5 mm were covered with 4.30 g of $NaNO_3$ (Fisher) in an alumina boat and heated to 350 °C for 67 h, after which the boat was allowed to cool slowly in the furnace. The crystals were worked up with hot water and filtered. The crystals were transparent, though larger ones were cracked, and all showed striae when viewed through crossed polars. Elemental analysis (Galbraith) gives a composition of $Na_{0.95}K_{0.05}TiPO_5$.

The high-temperature $Na_xK_{1-x}TiOPO_4$ phase space was investigated by grinding 5.00 mmol of TiO_2 with a total of 5.00 mmol of NaH_2PO_4 and KH_2PO_4 in different ratios, heating the mixture in a Pt crucible for 16 h at 600 °C, cooling, regrinding the sintered mass, and firing at 850 °C for 16 h.

A possible low-temperature route to direct Na substitution was investigated by crystallizing aqueous hydrogels containing $TiCl_4$ aqueous sol and varied concentrations of sodium and potassium phosphates at 200 °C and 15 bar. This method yielded crystalline powders, though no mixed-cation KTP isostructures were obtained. Starting Na:K ratios where Na/K < 1 gave only $KTiOPO_4$, and at higher Na/K ratios an unidentified phase resulted.

2.2.2. Characterization. All products were initially characterized by X-ray powder diffraction with a Scintag automated θ–θ powder diffractometer, using Cu Kα radiation (λ = 1.5418 Å). Lattice parameters with esd's were obtained on single-phase samples using Scintag software. All final crystallographic results (positions and temperature factors) reported in this work were obtained from single-crystal X-ray data. Routine data collection and refinement parameters for each compound are listed in Table I.

Prior to data collection, a single crystal of the desired phase was attached to a glass fiber with epoxy and mounted on an automated Huber four-circle X-ray diffractometer (graphite monochromated Mo Kα radiation, λ = 0.710 69 Å). The unit cell constants were determined from centered reflections and refined by least-squares analysis. Intensity data were collected using the θ–2θ scan method, with a scan rate of 6°/min from 1.3° below Kα_1 to 1.6° above Kα_2. Measurements were made out to 65° in 2θ. Three reflections were monitored every hundred observations. During data reduction, reflections were considered observed based on the criterion $I > 3\sigma(I)$. Observations were corrected for absorption analytically using the method of Busing and Levy.[27] In all refinements the KTP structure was used as a starting model in the space group $Pna2_1$. All least-squares and subsidiary calculations were performed using the Oxford CRYSTALS system.[28] An isotropic secondary extinction correction was included in the final cycles of refinement for most structures,[25] and the polarities of the structures were established unambiguously by refining the Flack enantiopole parameter.[29]

Powder SHG intensity data were collected at 1.064 μm using a system similar to that described by Dougherty and Kurtz.[30] Second harmonic (SH) light was collected in reflectance from samples of a uniform crystallite size between 1 and 3 μm, and intensities were measured relative to a quartz standard. A Spectra-Physics DCR11-3D Q-switched Nd:YAG laser was the source of the pump beam, producing 300-mJ, 8-ns pulses with a repetition rate of 2 Hz. SHG intensity was measured using a Tektronix 2467B 400 MHz oscilloscope with a DCS01 digitizing camera system.

2.2.3. Results. The (Na,K)$TiOPO_4$ compositions synthesized at high temperature crystallized in the KTP phase at Na concentrations between 0 and 65 mol %, and the products consist of solid solutions with the general formula $K_{1-x}Na_xTiOPO_4$. The two-phase region between 65 and 100 mol % Na contains $K_{0.35}Na_{0.65}TiOPO_4$ and α-$NaTiOPO_4$ in varying proportion. Lattice constants for the $K_{1-x}Na_xTiOPO_4$ (x = 0–1) compositions are reported in Table III. As Na replaces K in the $K_{1-x}Na_xTiOPO_4$ series,

(27) Busing, W.; Levy, H. *Acta Crystallogr.* **1957**, *10*, 180.
(28) Watkin, D. J.; Carruthers, J. R.; Betteridge, P. W. CRYSTALS *User Guide*; Chemical Crystallography Laboratory: Oxford, UK, 1985.
(29) Flack, H. D. *Acta Crystallogr.* **1983**, *A39*, 876.
(30) Dougherty, J. P.; Kurtz, S. K. *J. Appl. Crystallogr.* **1976**, *9*, 145.

Table III. Lattice Constants and SHG Intensities for MTiOPO$_4$ and MTiOAsO$_4$ Compounds

formula	*a*, Å	*b*, Å	*c*, Å	vol, Å^3	SHG/quartz
$KTiOPO_4$	12. 823 (4)	6.416 (6)	10.589 (3)	871.23	910
$Ag_{0.5}K_{0.5}TiOPO_4$	12.552	6.333	10.602	842.77	135
$Ag_{0.85}K_{0.15}TiOPO_4$	12.534 (2)	6.2939 (9)	10.524 (1)	830.21	7
$AgTiOPO_4$	12.524	6.263	10.530	825.95	5
$Na_{0.2}K_{0.8}TiOPO_4$	12.798 (9)	6.381 (5)	10.590 (6)	864.88	675
$Na_{0.4}K_{0.6}TiOPO_4$	12.79 (1)	6.343 (4)	10.57 (1)	857.57	620
$Na_{0.55}K_{0.45}TiOPO_4$	12.738 (4)	6.312 (3)	10.612 (4)	853.20	570
$Na_{0.65}K_{0.35}TiOPO_4$	12.734 (5)	6.313 (3)	10.613 (4)	853.13	590
$Na_{0.95}K_{0.05}TiOPO_4$	12.611 (2)	6.2810 (9)	10.595 (2)	839.23	90
$KTiOAsO_4$	13.146 (5)	6.584 (2)	10.771 (6)	932.35	990
$K_{0.13}Na_{0.87}TiOAsO_4$	12.8884 (9)	6.4095 (3)	10.7393 (6)	887.15	790

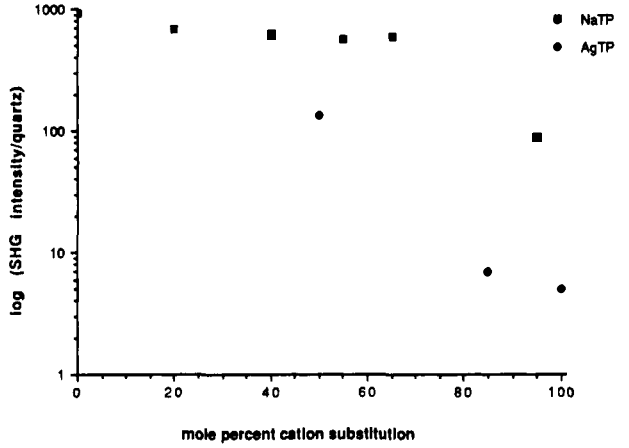

Figure 4. Powder SHG intensity vs composition for $Na_xK_{1-x}TiOPO_4$, $Ag_xK_{1-x}TiOPO_4$.

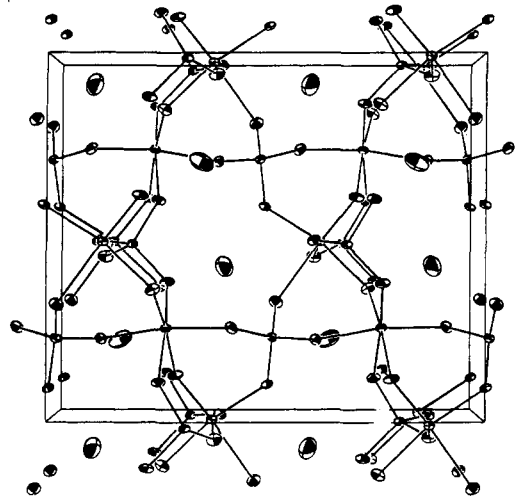

β-$NaTiOPO_4$ Orthorhombic $Pna2_1$

Figure 5. View of NaTP unit cell along [010].

the lattice constants *a* and *b* decrease by 1.55% and 1.92%, respectively, while *c* is reduced by only 0.29%. This anisotropic contraction may account for the striae seen in NaTP single crystals, as it should cause previously perfect crystals to break into mosaic blocks. The powder SHG intensities in this series drop slightly on initial substitution, remain steady until the limiting high-temperature composition $K_{0.35}Na_{0.65}TiOPO_4$ is reached, and then drop to one-tenth that of KTP in sodium-exchanged β-$NaTiOPO_4$ (Figure 4).

A 0.2 mm × 0.15 mm × 0.3 mm crystal of sodium-exchanged KTP with the formula $Na_{0.95}K_{0.05}TiOPO_4$ was used for single-crystal X-ray data collection. KTP atomic coordinates were used as a starting model and were refined to R = 5.39% (R_w = 5.41%). Structurally, NaTP is very

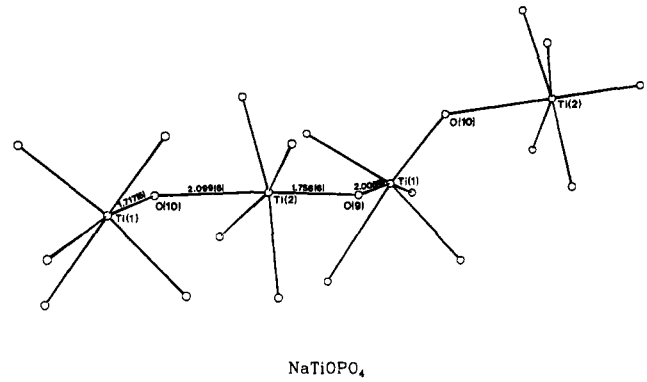

$NaTiOPO_4$

Figure 6. TiO_6 chain in NaTP, showing cis (Ti(1)) and trans (Ti(2)) linkages.

Table IV

(a) Final Atomic Positions and Thermal Parameters for NaTP

atom	*x*/*a*	*y*/*b*	*z*/*c*	*U*(equiv), Å^2
Na(1)	0.3485 (4)	0.7953 (7)	0.2904 (4)	0.0301
Na(2)	0.1004 (4)	0.747 (1)	0.0800 (5)	0.0380
Ti(1)	0.3728 (1)	0.5171 (2)	0.0091 (3)	0.0081
Ti(2)	0.23164 (9)	0.2853 (2)	0.2483 (3)	0.0086
P(1)	0.4842 (1)	0.3414 (3)	0.2762 (2)	0.0092
P(2)	0.1831 (1)	0.5198 (3)	0.5158 (2)	0.0079
O(1)	0.4754 (5)	0.519 (1)	0.1800 (5)	0.0134
O(2)	0.4960 (5)	0.442 (1)	0.4098 (5)	0.0113
O(3)	0.3839 (4)	0.2019 (9)	0.2799 (5)	0.0116
O(4)	0.5794 (4)	0.1937 (9)	0.2469 (6)	0.0117
O(5)	0.1164 (5)	0.3263 (9)	0.5522 (5)	0.0118
O(6)	0.1095 (4)	0.7109 (8)	0.5052 (5)	0.0110
O(7)	0.2673 (5)	0.551 (1)	0.6220 (5)	0.0118
O(8)	0.2447 (5)	0.489 (1)	0.3926 (5)	0.0105
O(9)	0.2584 (5)	0.4895 (9)	0.1394 (5)	0.0117
O(10)	0.2127 (5)	0.045 (1)	0.3841 (5)	0.0113

(b) Selected Bond Distances and Angles in NaTP

Distances, Å			
Ti(1)–O(1)	2.226 (6)	P(2)–O(5)	1.527 (6)
Ti(1)–O(2)	1.978 (6)	P(2)–O(6)	1.521 (5)
Ti(1)–O(5)	2.000 (6)	P(2)–O(7)	1.559 (6)
Ti(1)–O(6)	1.937 (5)	P(2)–O(8)	1.532 (6)
Ti(1)–O(9)	2.005 (6)		
Ti(1)–O(10)	1.717 (6)	Na(1)–O(1)	2.634 (7)
		Na(1)–O(3)	2.595 (7)
Ti(2)–O(3)	2.019 (5)	Na(1)–O(5)	2.569 (7)
Ti(2)–O(4)	1.924 (5)	Na(1)–O(7)	2.809 (8)
Ti(2)–O(7)	1.991 (6)	Na(1)–O(8)	2.568 (7)
Ti(2)–O(8)	1.999 (6)	Na(1)–O(9)	2.745 (8)
Ti(2)–O(9)	1.758 (6)	Na(1)–O(10)	2.525 (7)
Ti(2)–O(10)	2.099 (6)		
		Na(2)–O(1)	2.398 (8)
P(1)–O(1)	1.516 (6)	Na(2)–O(2)	2.493 (8)
P(1)–O(2)	1.557 (6)	Na(2)–O(5)	2.789 (8)
P(1)–O(3)	1.539 (5)	Na(2)–O(7)	2.571 (9)
P(1)–O(4)	1.549 (5)	Na(2)–O(9)	2.644 (8)

Angles, deg			
Ti(1)–O(9)–Ti(2)	130.8 (3)	O(9)–Ti(1)–O(10)	95.0 (3)
Ti(1)–O(10)–Ti(2)	132.3 (3)	O(9)–Ti(2)–O(10)	175.2 (3)

Table V

(a) Final Atomic Positions and Thermal Parameters for AgTP

atom	x/a	y/b	z/c	U(equiv), Å²
Ag(1)	0.3538 (2)	0.8121 (3)	0.3020 (4)	0.0327
Ag(2)	0.1111 (1)	0.7428 (3)	0.1106 (5)	0.0412
K(1)	0.3538 (2)	0.8121 (3)	0.3020 (4)	0.0327
K(2)	0.1111 (1)	0.7428 (3)	0.1106 (5)	0.0412
Ti(1)	0.3724 (2)	0.5325 (4)	0.0067 (4)	0.0109
Ti(2)	0.2240 (2)	0.2944 (4)	0.2392 (4)	0.0103
P(1)	0.4781 (3)	0.3426 (6)	0.2762 (4)	0.0111
P(2)	0.1823 (3)	0.5358 (6)	0.5094 (4)	0.0098
O(1)	0.4716 (8)	0.532 (2)	0.182 (1)	0.0130
O(2)	0.4902 (9)	0.427 (2)	0.413 (1)	0.0153
O(3)	0.3734 (8)	0.210 (2)	0.272 (1)	0.0159
O(4)	0.5727 (7)	0.192 (2)	0.238 (1)	0.0105
O(5)	0.1179 (9)	0.340 (1)	0.549 (1)	0.0108
O(6)	0.1068 (7)	0.728 (2)	0.504 (1)	0.0061
O(7)	0.2728 (9)	0.571 (2)	0.606 (1)	0.0133
O(8)	0.236 (1)	0.507 (2)	0.380 (1)	0.0075
O(9)	0.2505 (8)	0.501 (2)	0.128 (1)	0.0132
O(10)	0.2056 (9)	0.058 (2)	0.374 (1)	0.0123

(b) Selected Bond Distances and Angles in AgTP

Distances, Å

Ti(1)–O(1)	2.23 (1)	P(2)–O(5)	1.53 (1)
Ti(1)–O(2)	2.00 (1)	P(2)–O(6)	1.53 (1)
Ti(1)–O(5)	1.99 (1)	P(2)–O(7)	1.54 (1)
Ti(1)–O(6)	1.94 (1)	P(2)–O(8)	1.53 (1)
Ti(1)–O(9)	2.00 (1)		
Ti(1)–O(10)	1.71 (1)	Ag(1)–O(1)	2.62 (1)
		Ag(1)–O(3)	2.53 (1)
Ti(2)–O(3)	1.98 (1)	Ag(1)–O(5)	2.69 (1)
Ti(2)–O(4)	1.899 (9)	Ag(1)–O(8)	2.56 (1)
Ti(2)–O(7)	1.99 (1)	Ag(1)–O(9)	2.98 (1)
Ti(2)–O(8)	2.00 (1)	Ag(1)–O(10)	2.54 (1)
Ti(2)–O(9)	1.78 (1)		
Ti(2)–O(10)	2.07 (1)	Ag(2)–O(1)	2.37 (1)
		Ag(2)–O(2)	2.70 (1)
P(1)–O(1)	1.55 (1)	Ag(2)–O(5)	2.99 (1)
P(1)–O(2)	1.54 (1)	Ag(2)–O(7)	2.53 (1)
P(1)–O(3)	1.56 (1)	Ag(2)–O(9)	2.33 (1)
P(1)–O(4)	1.57 (1)		

Angles, deg

Ti(1)–O(9)–Ti(2)	129.5 (6)	O(9)–Ti(1)–O(10)	95.3 (5)
Ti(1)–O(10)–Ti(2)	133.8 (6)	O(9)–Ti(2)–O(10)	175.4 (5)

similar to KTP (Figure 5), and in particular the coordination environments around the Ti and P atoms are nearly identical, with the TiO_6 octahedra connected alternately by *cis*-O(9)–Ti(1)–O(10) and *trans*-O(9)–Ti(2)–O(10) links (Figure 6). Again, the short Ti(1)–O(10) and Ti(2)–O(9) bonds are trans to long Ti–O bonds. Relevant bond distances and angles are presented in Table IVb. Exchange of Na for K induces no significant alteration of these distances versus those of KTP. Therefore, unlike previously reported KTP isostructures with weak SHG intensities, *the loss of SHG intensity in NaTP cannot be accounted for in terms of Ti–O coordination distances alone.* The possibility of the decrease in SHG intensity being due to changes in orientation of the TiO_6 octahedra is described in section 5.

We note here that these results are entirely consistent with the results obtained for KTP and KTA from single-crystal NLO and structural data. The TiO_6 octahedra in KTA are less distorted than those in KTP, and the orientations of the TiO_6 groups in these two structures as determined by the direction cosines of Ti(1)–O(10) and Ti(2)–O(9) (with respect to the *z* axis) are within 2.0° (Table VII). Nevertheless, measurements of NLO coefficients on single crystals of $KTiOAsO_4$ show that KTA's effective type II doubling coefficient is 60% larger than that of KTP.[6]

Of particular significance are the coordination numbers of Na(1) and Na(2) which at seven and five (within 2.95 Å), respectively, are significantly lower than those of K(1) and K(2) in KTP (8 and 9). This result indicates that though K^+ has been replaced by a smaller cation, the channel diameter remains approximately the same in NaTP and KTP, and the Na^+ ions can find fewer oxygen atoms within 3.0 Å to coordinate with. One can infer that the KTP/NaTP framework is fairly rigid and that the cations provide only secondary structural support. Other features of interest include the Ti(1)–O(9)–Ti(2) bond angle which, at 130.8°, is unusually small compared with 135.5° for the same angle in KTP. The close coordination of both Na(1) and Na(2) to O(9) may be responsible. It was not possible to reliably determine whether selective siting between the two crystallographically nonequivalent cation sites occurs for Na and K due to the low concentration of the latter.

Table VI

(a) Final Atomic Positions and Thermal Parameters for NaTA

atom	x/a	y/b	z/c	U(equiv), Å²
Na(1)	0.3388 (6)	0.8071 (9)	0.2813 (5)	0.0469
Na(2)	0.0941 (5)	0.727 (1)	0.0982 (6)	0.0481
K(1)	0.3388 (6)	0.8071 (9)	0.2813 (5)	0.0469
K(2)	0.0941 (5)	0.727 (1)	0.0982 (6)	0.0481
Ti(1)	0.3758 (1)	0.5361 (2)	0.0064 (2)	0.0107
Ti(2)	0.2246 (1)	0.2985 (3)	0.2369 (2)	0.0122
As(1)	0.47800 (7)	0.3282 (1)	0.2743 (2)	0.0119
As(2)	0.18583 (7)	0.5381 (1)	0.5099 (2)	0.0116
O(1)	0.4716 (6)	0.539 (1)	0.1824 (7)	0.0173
O(2)	0.4892 (6)	0.408 (1)	0.4242 (7)	0.0166
O(3)	0.3690 (5)	0.186 (1)	0.2674 (7)	0.0114
O(4)	0.5754 (5)	0.162 (1)	0.2373 (7)	0.0147
O(5)	0.1190 (6)	0.330 (1)	0.5579 (7)	0.0157
O(6)	0.1013 (6)	0.738 (1)	0.5004 (7)	0.0159
O(7)	0.2842 (6)	0.568 (1)	0.6127 (7)	0.0174
O(8)	0.2441 (6)	0.510 (1)	0.3677 (6)	0.0151
O(9)	0.2575 (6)	0.490 (1)	0.1238 (7)	0.0170
O(10)	0.1964 (6)	0.070 (1)	0.3736 (6)	0.0143

(b) Selected Bond Distances and Angles in NaTA

Distances, Å

Ti(1)–O(1)	2.257 (8)	As(2)–O(5)	1.667 (7)
Ti(1)–O(2)	1.982 (7)	As(2)–O(6)	1.683 (7)
Ti(1)–O(5)	1.967 (8)	As(2)–O(7)	1.693 (8)
Ti(1)–O(6)	1.937 (7)	As(2)–O(8)	1.712 (7)
Ti(1)–O(9)	2.001 (8)		
Ti(1)–O(10)	1.718 (7)	Na(1)–O(1)	2.65 (1)
		Na(1)–O(3)	2.462 (9)
Ti(2)–O(3)	2.024 (7)	Na(1)–O(5)	2.46 (1)
Ti(2)–O(4)	1.939 (7)	Na(1)–O(7)	2.93 (1)
Ti(2)–O(7)	1.992 (8)	Na(1)–O(8)	2.45 (1)
Ti(2)–O(8)	1.967 (7)	Na(1)–O(9)	2.84 (1)
Ti(2)–O(9)	1.777 (8)	Na(1)–O(10)	2.68 (1)
Ti(2)–O(10)	2.103 (7)		
		Na(2)–O(1)	2.36 (1)
As(1)–O(1)	1.673 (8)	Na(2)–O(2)	2.45 (1)
As(1)–O(2)	1.696 (7)	Na(2)–O(4)	2.92 (1)
As(1)–O(3)	1.677 (7)	Na(2)–O(5)	2.80 (1)
As(1)–O(4)	1.693 (7)	Na(2)–O(7)	2.69 (1)
		Na(2)–O(9)	2.61 (1)

Angles, deg

Ti(1)–O(9)–Ti(2)	135.6 (5)	O(9)–Ti(1)–O(10)	97.4 (4)
Ti(1)–O(10)–Ti(2)	139.6 (5)	O(9)–Ti(2)–O(10)	176.1 (3)

Table VII lists average cation–oxygen distances for KTP, KTA, and the three KTP-type structures reported in this work. The average cation–oxygen distances in NaTA, at 2.64 Å for Na(1) and 2.58 Å for Na(2), are less than those in KTP ($K(1)$ = 2.84 Å, $K(2)$ = 2.93 Å) and KTA ($K(1)$ = 2.87 Å, $K(2)$ = 2.95 Å). However, the relative affinities of the Na^+ ions for the two chemically distinct oxygen atoms in the structure, the phosphate oxygens (O(1)–O(8)) and the titanyl or bridging oxygens (O(9) and O(10)), are nearly the same as measured by cation–oxygen bond valences (Table VIII).[31] It is worth noting here that despite

Table VII. Crystallographic Summary

	KTP	KTA	AgTP	NaTP	NaTA
Bond Distances, Å					
Ti(1)–O(1)	2.161 (4)	2.14 (1)	2.23 (1)	2.226 (6)	2.257 (8)
Ti(1)–O(9)	1.993 (4)	1.96 (2)	2.00 (1)	2.005 (6)	2.001 (80
Ti(1)–O(10)	1.718 (4)	1.74 (2)	1.71 (1)	1.717 (6)	1.718 (7)
ΔTi(1)	0.443 (6)	0.40 (2)	0.54 (1)	0.509 (8)	0.54 (1)
Ti(2)–O(9)	1.738 (4)	1.77 (2)	1.78 (1)	1.758 (6)	1.777 (8)
Ti(2)–O(10)	2.101 (4)	2.09 (2)	2.07 (1)	2.099 (6)	2.103 (7)
ΔTi(2)	0.363 (6)	0.33 (3)	0.29 (1)	0.341 (8)	0.33 (1)
Bond Angles, deg					
O(1)–Ti(1)–O(10)	172.2	171.8	1.754 (5)	172.9 (4)	173.4 (3)
O(9)–Ti(1)–O(10)	94.8	94.8	95.3 (5)	95.0 (3)	97.4 (4)
O(9)–Ti(2)–O(10)	174.7	175.5	175.4 (5)	175.2 (3)	176.1 (3)
Ti(1)–O(9)–Ti(2)	135.5	137.2	129.5 (6)	130.8 (3)	135.6 (5)
Ti(1)–O(10)–Ti(2)	132.9	135.2	133.8 (6)	132.3 (3)	139.6 (5)
Direction Cosines					
Ti(1)–O(10)	0.667	0.693	0.816	0.769	0.830
Ti(2)–O(9)	0.652	0.669	0.661	0.654	0.683
Coordination Numbers					
cation 1	8	8	5	7	7
cation 2	9	9	4	5	6
Average Cation–Oxygen Distance, Å					
	2.89	2.91	2.54	2.61	2.64

the similarities in their average K–O distances, bond valence calculations show that KTP and KTA differ in the affinity of the cations for the titanyl oxygen atoms versus the phosphate or arsenate oxygen atoms. This may be due to the increased basicity of arsenate oxygens, which draw the K^+ ions away from the bridging oxygens to a greater degree in KTA.

Because the metal–oxygen distances in the TiO_6 octahedra in NaTP and KTP are nearly identical, it is difficult to understand the loss of SHG intensity in NaTP in terms of schemes which model hyperpolarizability only in terms of bonding in localized MO_6 units. The cations must become involved, either by altering the titanyl chain electronic states or by causing the TiO_6 groups to reorient in an unfavorable way. These topics are addressed in section 5.

3. Silver Titanyl Phosphate ($AgTiOPO_4$)

The smaller size and greater electronegativity of silver (versus potassium), coupled with its preference for lower coordination numbers than alkali-metal cations makes it likely that the cation–framework bonding in AgTP differs from KTP in a fashion similar to that in NaTP. If this interaction is stronger than in NaTP and if cation coordination can influence titanyl chain hyperpolarizability, then we should expect AgTP's SHG intensity to be even weaker than NaTP's.

3.1. Experimental Part. The KTP crystals used for Ag exchange were identical to those used in NaTP synthesis (section 2.1). Flux-grown KTP crystals (0.216 g) between 0.5 and 1 mm diameter were heated with 5.00 g of a 50–50 wt % $AgNO_3$–$AgClO_3$ mixture (mp = 143 °C) in a porcelain crucible at 185 °C for 40 h. After cooling the melt in the furnace, the silver salts were dissolved away with hot water, and the crystals were recovered by filtration. To dissolve any AgCl which may have formed from decomposition of $AgClO_3$ the crystals were washed with 20 mL of 1 M NH_3(aq) solution, rinsed with water and methanol, and air dried; 0.278 g was recovered. The smaller crystals used for structure determination were transparent with striae visible through crossed polars. Elemental analysis (Galbraith) gave a formula of $Ag_{0.85}K_{0.15}TiPO_5$. The exchange procedure was repeated at higher and lower temperatures to give different silver concentrations; the lattice constants for each product are given in Table III.

The limits of direct Ag substitution were determined by grinding 0.400 g (5 mmol) of TiO_2 with a total of 5 mmol of KH_2PO_4 and equimolar quantities of $AgNO_3$ and $NH_4H_2PO_4$ in several different proportions, heating the mixtures in Pt crucibles at 600 °C for 16 h, cooling, and twice regrinding and refiring the sintered masses at 850 °C for 16 h.

Procedures for SHG intensity and powder and single-crystal X-ray data collection are the same as those outlined for NaTP in section 2.1. Results from crystallographic data collection and reduction on $Ag_{0.85}K_{0.15}TiOPO_4$ are listed in Table I.

3.2. Results. Melt temperatures between 165 and 185 °C gave products with essentially the same unit cell volume and similar compositions. Fully exchanged AgTP can be prepared by melting a large (>100-fold) molar excess of $AgNO_3$ over KTP powder or crystals between 225 and 275 °C, but crystals so treated became cracked and opaque. The lattice constants for $AgTiOPO_4$ show that the unit cell shrinks anisotropically during exchange: a is reduced by 2.27%, b by 2.20%, and c by only 0.81%. As with NaTP, this may account for both the striae seen under crossed polars and the ω widths (0.30°) of some of the peaks seen during single-crystal data collection on $Ag_{0.85}K_{0.15}TiOPO_4$.

The mobility of the silver ions in AgTP is seen in its reactivity was well as its synthesis. For example, if AgKTP crystals are treated with a mild reducing agent such as hydrazine hydrate or hydroquinone, the surfaces of the crystals turn black from metallic silver. AgTP powder treated with aqueous KCN becomes amorphous due to loss of the cation to form $Ag(CN)_2^-$. Exposing KTP crystals to 10 M $AgNO_3$(aq) at 200 °C results in no exchange, which can be attributed to a larger hydrated Ag^+ ion radius versus that of unhydrated ions in a nonaqueous melt.

Formulas of the ion-exchanged materials were established by applying Vegard's law to cell volumes. The limit of Ag substitution through high-temperature synthesis apparently occurs near the composition $Ag_{0.50}K_{0.50}TiOPO_4$. Direct combination of $AgNO_3$, $NH_4H_2PO_4$, and TiO_2 in equimolar quantities at high temperature results in a polymorph of $AgTiOPO_4$ isostructural with α-$NaTiOPO_4$, termed α-$AgTiOPO_4$.

SHG intensities relative to quartz for $AgTiOPO_4$ and $Ag_xK_{1-x}TiOPO_4$ compounds prepared by ion exchange are listed in Table III. Complete Ag substitution in KTP is accompanied by reduction of SHG intensity to only 5 times that of quartz, the lowest value reported for any Ti-containing KTP isostructure. This value is approximately the same as that of $(NH_4)_{0.5}H_{0.5}TiOPO_4$ (6 times quartz), in which the loss of 0.5 equiv of NH_3 from NH_4TiOPO_4 results in a lengthening of the previously short Ti(1)–O(10) bond to a distance more characteristic of a Ti–O "long bond". This increase is associated with a reduction of the Ti(1)–O(9)–Ti(2) bond angle, which is thought to be caused by protonation of O(9).[32] The similar SHG intensity of AgTP therefore invites speculation that an analogous mechanism involving strong silver–oxygen bonding may be responsible.

Following data reduction and using the KTP starting model, the structure of $Ag_{0.85}K_{0.15}TiOPO_4$ was refined to R = 5.03% (R_w = 5.06%). The AgTP structure is illustrated in Figure 7. Two oxygen atoms in the asymmetric

(31) Brown, I. D.; Wu, K. K. *Acta Crystallogr.* **1976**, *B32*, 1957.

(32) Eddy, M. M.; Gier, T. E.; Keder, N. L.; Stucky, G. D.; Cox, D. E.; Bierlein, J. D.; Jones, G. *Inorg. Chem.* **1988**, *27*, 1856.

Table VIII. Metal–Oxygen Bond Distances (Å) and Valences in KTP Isostructures

	KTP		KTA		NaTP		AgTP		NaTA		NHTP	
bond	dist	valence	dist	valence	dist	valence	dist	valence	dist	valence	dist	valence
Ti(1)–O(1)	2.161	0.393	2.138	0.416	2.226	0.337	2.23	0.334	2.257	0.314	1.947	0.676
Ti(1)–O(2)	1.957	0.659	1.947	0.676	1.978	0.623	2.00	0.588	1.982	0.617	1.926	0.716
Ti(1)–O(5)	2.047	0.521	2.002	0.585	2.000	0.588	1.99	0.603	1.967	0.641	1.915	0.737
Ti(1)–O(6)	1.900	0.768	2.004	0.582	1.937	0.695	1.94	0.689	1.937	0.695	1.950	0.671
Ti(1)–O(9)	1.993	0.599	1.957	0.659	2.005	0.581	2.00	0.588	2.001	0.587	2.012	0.570
Ti(1)–O(10)	1.718	1.297	1.735	1.232	1.717	1.301	1.71	1.328	1.718	1.297	1.903	0.762
Ti(2)–O(3)	2.037	0.535	2.025	0.551	2.019	0.560	1.98	0.620	2.024	0.553	1.984	0.613
Ti(2)–O(4)	1.979	0.621	1.989	0.605	1.924	0.720	1.90	0.770	1.939	0.691	1.996	0.594
Ti(2)–O(7)	1.966	0.643	1.941	0.687	1.991	0.602	1.99	0.604	1.992	0.601	1.957	0.659
Ti(2)–O(8)	1.994	0.598	1.983	0.615	1.999	0.590	2.00	0.588	1.967	0.641	1.982	0.617
Ti(2)–O(9)	1.738	1.221	1.770	1.110	1.758	1.150	1.78	1.078	1.777	1.088	2.114	0.441
Ti(2)–O(10)	2.101	0.455	2.097	0.460	2.099	0.458	2.07	0.492	2.103	0.453	1.761	1.140
Ti(1) atomic valence		4.237		4.150		4.125		4.132		4.150		4.133
Ti(2) atomic valence		4.073		4.029		4.080		4.152		4.027		4.064
O(9) atomic valence		2.074		1.942		1.959		1.973		1.895		1.080
O(10) atomic valence		2.020		1.877		1.908		1.960		1.866		2.033
	av dist	av valence	av dist	av valence	av dist	av valence	av dist	av valence	av dist	av valence	av dist	av valence
M(1)–O(1-8)	2.843	0.142	2.83	0.162	2.635	0.126	2.60	0.089	2.59	0.141	2.98	0.095
M(1)–O(9,10)	2.852	0.142	2.99	0.091	2.635	0.127	2.54	0.091	2.76	0.103	2.95	0.100
M(2)–O(1-8)	2.941	0.110	2.93	0.129	2.563	0.145	2.53	0.108	2.64	0.132		
M(2)–O(9,10)	2.910	0.119	3.00	0.089	2.644	0.123	2.33	0.264	2.61	0.130		

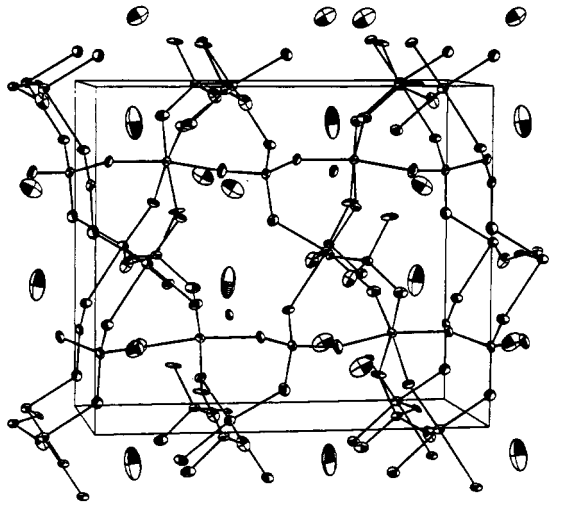

$(Ag_{0.85}K_{0.15})TiOPO_4$

Figure 7. Oblique view of AgTP (010) plane.

unit are coordinated to the crystallographically inequivalent Ti atoms with alternately long (2.00, 2.07 Å) and short (1.71, 1.78 Å) bond distances. As is the case in NaTP, exchange of Ag for K induces no significant alteration of the Ti–O bond distances versus those of KTP (Table VII).

Other interesting structural features of AgTP include selective siting by the Ag and K atoms on the two crystallographically nonequivalent cation positions in the asymmetric unit. The occupancy of silver on Ag(1) is 70% and 100% on Ag(2). Using the same maximum bond length criterion as for sodium (2.95 Å) the coordination numbers of silver in AgTP are five and four, or even less than those in NaTP. This result is in line with our predictions of the Ag coordination environment based on silver's predilection for low coordination numbers and again reflects the secondary role the cation plays in structurally supporting the KTP framework.

As is observed in both NaTP and NHTP, the Ti(1)–O(9)–Ti(2) bond angle in AgTP is reduced, in this case from 135.5° (in KTP) to 129.5°.[33] Interestingly, the Ag(2)–O(9) distance at 2.33 Å is the shortest silver–oxygen contact in the AgTP structure, suggesting that the influence of the strong coordination of Ag(2) to O(9) is similar to that of the proton in NHTP, though in this case the Ti(1)–O(10) bond is not lengthened. The average Ag–O distances, 2.59 Å for Ag(1) and 2.48 Å for Ag(2), are shorter than the average Na–O distances in NaTP, but more striking is the difference in the relative affinities of the Ag^+ ions for the titanyl and phosphate oxygen atoms (Table VIII). In particular, the Ag(2)–O(9) bond valence is nearly 2.5 times that of the average silver–phosphate oxygen valence.

This result shows that silver is very strongly associated with the titanyl chain in AgTP, more so than the cations in either NaTP of KTP, with a concomitant reduction in SHG intensity. Again, this influence may be manifesting itself as a perturbation of electronic states in the TiO_6 groups or as a subtle realignment of framework geometry (see section 5).

4. Sodium Titanyl Arsenate ($NaTiOAsO_4$)

From the preceding discussions of NaTP and AgTP it should be evident that the stability of the framework and the mobility of these small cations allow ion exchange to take place to completion or near completion whether or not these same materials can be prepared from direct methods. Though the ion mobility in KTA is less than in KTP as measured by ac conductivity[6] it is not unreasonable to expect that exchange for smaller cations should take place. The nature of the cation–framework interaction in KTA need not necessarily be directly analogous to that in KTP, and measuring such properties as cation site selectivity and SHG intensity would provide more insight into this interaction than can be obtained by studying $MTiOPO_4$ compounds alone.

4.1. Experimental Part. KTA crystals were grown hydrothermally: 0.080 g TiO_2, 1.26 g KH_2AsO_4, 0.28 mL of 5.00 N KOH solution, and 0.50 mL of H_2O were sealed inside a 0.25-in.-o.d. gold tube 3.00 in. long. The tube was placed inside a water-filled Leco Tem-Pres bomb which was then pressurized to 20 000 psi and heated. After reaching 675 °C and 45 000 psi, no external controls were placed on pressure. The bomb was held at this temperature for 8 h, then cooled to 450 °C over 100 h, and then cooled to 350 °C over 20 h. Upon reaching 350 °C the

(33) KTP and NHTP results were taken from refs 7 and 32.

bomb was allowed to cool to room temperature. The gold tube was cut open and the contents were rinsed out and filtered. Yield was 0.220 g of KTA crystals ranging in diameter from 0.050 and 1 mm.

In a 30-mL Pyrex beaker, 2.5 g of $NaNO_3$, 2.5 g of $NaNO_2$, and 2.5 g of $CH_3COONa{\cdot}3H_2O$ were heated to 250 °C until all contents were molten and boiling had ceased. A portion of the above KTA crystals (0.064 g) was added to the hot melt which was maintained at 215 °C for 65 h. The melt was then allowed to cool in the furnace, and the crystals were recovered by soaking in hot water and filtering. Yield was 0.060 g. The larger crystals were white, slightly translucent pieces; the smaller crystals were transparent but contained the striae seen in NaTP and AgTP. Elemental analysis for Na and K (Galbraith) gave a composition of $Na_{0.87}K_{0.13}TiAsO_5$.

The high-temperature $K_{1-x}Na_xTiOAsO_4$ phase space was investigated by reacting 0.400 g of TiO_2 and 0.795 g of $NH_4H_2AsO_4$ (5.00 mmol each) with a total of 5.00 mmol of $KHCO_3$ and $NaHCO_3$ in different ratios. The starting materials were ground together, heated in Pt crucibles at 650 °C for 16 h, cooled, reground, and reheated at 850 °C for another 16 h. Products were characterized by powder X-ray diffraction.

X-ray crystallographic results from data acquisition and reduction on NaTA are given in Table I. Powder SHG intensity data were obtained from NaTA in the same fashion as NaTP and AgTP, using crystals of approximately 3-μm diameter.

4.2. Results. The anisotropy of the unit-cell contraction is more pronounced in NaTA than in any other $MTiOXO_4$ compound studied: a and b both shrink by approximately 2%, while the c axis length contracts by only 0.06%. As a result the NaTA crystals appear highly mosaic under crossed polars.

No more than 20 mol % Na could be accommodated in the KTP structure through direct synthesis at 850 °C. Combining equimolar quantities of TiO_2, $NaHCO_3$, and $NH_4H_2AsO_4$ at 850 °C yields a phase isomorphous with α-$NaTiOPO_4$. The two-phase region between 20 and 100 mol % Na contains $K_{0.8}Na_{0.2}TiOAsO_4$ and the titanite phase in varying proportion. Thus NaTA lies even further outside the high-temperature KTP phase space than either AgTP or NaTP, as we might expect from the larger size of the framework compared with the cation radius. Lattice constants for both $K_{0.8}Na_{0.2}TiOAsO_4$ and $K_{0.13}Na_{0.87}TiOAsO_4$ are given in Table III.

Using single-crystal diffraction data from $K_{0.13}Na_{0.87}TiOAsO_4$, a starting model consisting of KTA structure coordinates and temperature factors was refined to R = 6.22% (R_w = 6.39%). NaTA and KTA are isostructural (Figure 8), and the Ti coordination environments in NaTA differ little from those in KTA or KTP. Fractional coordinates and isotropic thermal parameters are given in Table VIa, and pertinent bond distances and angles are listed in Table VIb. The Ti(1)–O(10) bond, at 1.718 Å, is actually slightly shorter than the same bond in KTA (1.735 Å), though the Ti(2)–O(9) bonds are nearly the same length in both compounds (1.777 vs 1.770 Å in KTA). The Ti(1)–O(9)–Ti(2) bond angle, 135.6°, is disturbed little from its value in KTA (137.2°).

The coordination numbers (CN) of Na are 7 and 6 for Na(1) and Na(2) (within 2.95 Å) and are thus higher than those in NaTP (CN = 6 and 5). The difference in the populations of Na and K in each cation site from the overall stoichiometry is not statistically significant. The average Na–O distance in NaTA, 2.64 Å, is essentially the same as NaTP's (2.61 Å). The difference again lies in the relative affinities of the Na^+ ions for the titanyl and the arsenate oxygen atoms. Comparing Na–O bond valences for the two types of interactions shows that as is the case in KTA, the increased basicity of the arsenate oxygen atoms draws the cations away from the titanyl oxygen atoms (Table VIII). The net effect is a weaker coordination of the Na^+ ion to the titanyl chain in the NaTA structure than in NaTP or AgTP.

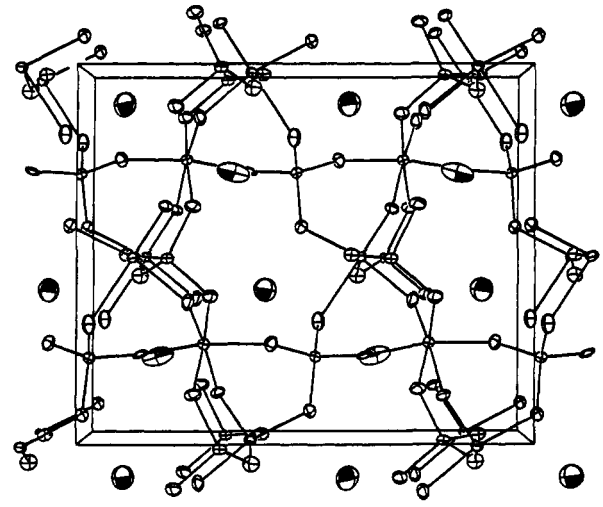

$(Na_{0.87}K_{0.13})TiOAsO_4$

Figure 8. View of NaTA unit cell along [010].

The powder SHG intensity of NaTA is about 80% that of KTA or KTP, or much greater than that of either NaTP or AgTP. This result, combined with the low affinity of the Na ions for the oxygen atoms in the Ti–O chain, completes the trend seen in these three compounds.

5. Discussion

Several patterns have emerged from our study of these compounds. First, cation exchange does not necessarily structurally perturb the framework sufficiently to alter Ti–O or P–O distances, even if the cation is so small as to render the resulting structure thermodynamically unfavorable. Second, the smaller Ag and Na ions have lower coordination numbers in this structure than do potassium ions. Third, strong cation–oxygen interactions are associated with loss of SHG intensity.

Table VII lists key crystallographic results for the three compounds reported in this work, plus KTP and KTA. A common theme in NaTP, NHTP, and AgTP is the association between cation exchange/desorption and both loss of SHG intensity and perturbation of the Ti(1)–O(9)–Ti(2) bond angle. This effect is seen to its greatest extent in NHTP, in which this angle is reduced to 127.4°, and it is implicated in the lengthening of the Ti(1)–O(10) bond as well. An unusual degree of basicity of this oxygen atom may be responsible for its affinity for cations.

To quantify the cation's influence on electron density in the Ti–O bonds, bond orders were calculated for the Ti–O bonds in NaTP, AgTP, NaTA, KTP, KTA, and NHTP using the bond valence parameters of Brown and Wu (Table VIII).[31] Note that the short bonds in KTP (Ti(1)–O(10) and Ti(2)–O(9)) have bond orders approximately twice those of the other Ti–O bonds, indicating the short Ti=O interactions represent true "double bonds". For all compounds the Ti valences, which are the sums of the bond orders for a particular Ti atom, equal 4, which is what is expected for tetravalent Ti. In NHTP the Ti(1)–O(10) bond has been lengthened to 1.9 Å, and this is accompanied by a reduction in bond order to a single bond

value. Examining the valences of O(9) (calculated by summing the Ti(1)–O(9) and Ti(2)–O(9) bond orders) for KTP and NHTP, we see that this value has been reduced from nearly 2 (1.82) in the former to 1.0 in the latter. This supports the assertion that the proton in NHTP is bonding with O(9), simultaneously reducing its valence to what is expected for a hydroxyl group. The concomitant reduction of the order of Ti(1)–O(10) from that of a double bond to that of a single bond may explain the lost Ti–O bond hyperpolarizability as seen in the attenuation of SHG intensity.

A similar effect on the O(9) valence takes place to a lesser extent in AgTP (1.67) and NaTP (1.73). NaTA has an even lower O(9) valence (1.60); however, this compound has a much greater SHG intensity than either AgTP or NaTP, and the trend relating low O(9) valence and low SHG intensity is lost. It should be remembered, though, that this method is based entirely on Ti–O bond distances and that the cations may be affecting metal–oxygen bond polarizabilities in more subtle ways. For example, coordination of alkali-metal cations to the essentially nonbonding oxygen lone pair electrons may have a larger effect on polarizability than on Ti–O bond lengths.

It is conceivable that differences in NLO susceptibility among KTP isostructures could be caused not only by changes in Ti–O distances, but by changes in the relative orientations of the TiO_6 octahedra. In an extreme situation these groups could reorient such that their β_{ijk} values cancel, leaving little or no net contribution to $\chi^{(2)}$. Before such changes can be established, the orientation of a TiO_6 group must be defined. In all KTP isostructures which crystallize in the space group $Pna2_1$ the x and y components of any particular short Ti=O bond are exactly cancelled by components of equal magnitude and opposite sign from other Ti=O bonds in the unit cell. Table VII lists the angles the axes of the two short Ti=O bonds make with respect to [001], expressed as direction cosines. This selection is justified by relevance of these bonds to the β_{ijk} values of the TiO_6 units and by the lack of sizable differences in O–Ti–O angles within the TiO_6 units between isostructures.

The cosines of the Ti(1)–O(10) bonds are all greater in the exchanged structures than in KTP, meaning this bond is more aligned with the z axis in these compounds than in KTP. Little trend is noticeable in the cosines of the Ti(2)–O(9) bonds in KTP, NaTP, AgTP, and NaTA. If we assume that the direction cosine of Ti(1)–O(10) in KTP (0.667) represents a near-optimum angle, it is tempting to suspect that the decreased angles in NaTP (0.816) and AgTP (0.769) are related to their diminished SHG intensities. However, the value of this cosine in NaTA is even greater (0.830), and therefore no trend exists. It is thus unlikely that rearrangements of framework geometry on the scale displayed in these compounds can be exclusively responsible for changes in NLO characteristics, though minor influences cannot be ruled out.[34]

Levine's theory (section 1.2) accounts for KTP's NLO susceptibility in terms of Ti–O distances alone and clearly cannot model the observed optical data. Chen's anionic group model explicitly assigns NLO response in ferroelectric metal oxides to the MO_6 group and its structural distortions without any significant contributions from other framework cations (e.g., K and P). This model is also clearly inadequate for the KTP structural family.

In ferroelectric metal oxides the metal coordination sphere distorts via a second-order Jahn–Teller effect, which stabilizes the bonding (occupied) orbitals, which are of mostly oxygen character, at the expense of the antibonding (empty) orbitals, which are of metallic character and thus constitute a charge-transfer excited state.[35] This distortion results in the mixing of charge-transfer character into both the bonding orbitals and the nonbonding oxygen lone-pair orbitals, which constitute the HOMOs. The anharmonicity in these electronic potentials depends on the degree to which charge-transfer character can be mixed into these ground-state orbitals. A similar argument used to rationalize large β_{ijk} values in organic molecules that contain donor and acceptor functional groups separated by a conjugated π system correlates strong second-order polarizability with large π^* excited-state dipole moments.[36]

Earlier studies of the KTP isomorph potassium vanadyl phosphate (KVP) demonstrate an extensively delocalized excited state.[37] This agrees with the results of Brixner and Blasse,[38] who have confirmed that the delocalized charge-transfer state in KTP is semiconductor-like in nature. Excited-state charge transfer with the bridging oxygen atoms in the KTP titanyl chain has also been identified by Jarman et al. using ab initio Hartree–Fock calculations on isolated $Ti(OH)_4O_2^{4-}$ groups.[39]

Delocalization would result in a high degree of polarization with unusually large excited-state dipole moment contributions. We suggest that this is the most important consideration in understanding the NLO behavior of KTP, i.e., that the charge-transfer excited state is delocalized along the TiO_6 chains and thus represents a conduction band. To fully understand KTPs optical properties, it will be necessary to treat the electronic states in terms of a delocalized band structure model.

We have previously discussed how mixing coefficients in KTP may be altered both by influences internal and external to the metal coordination sphere.[37] Increased bandgap energy (E_g), caused by substituting d^{10} metal ions such as Ga, Ge, and Sn onto the octahedral sites, has a significant effect on distortion and thus on mixing and excited-state delocalization, resulting in sharp attenuation in NLO susceptibility.[40,41] Replacing As for the more electronegative P on the tetrahedral sites increases the coordination strength of the exchangeable cation to the XO_4 (X = P, As) oxygen atoms and correspondingly decreases the strength of the interaction of the cation to the $[Ti–O]_n$ chain oxygen atoms. This decreased "pinning" of the delocalized excited state (and smaller bandgap) would explain the observed improvement in doubling efficiency of KTA over KTP as determined by single-crystal SHG measurements. A related effect is the loss of microscopic susceptibility which takes place as the interactions between the cations and framework oxygen levels become more covalent. This occurs when low-coordinate and/or highly electronegative cations cause the occupied TiO_6 orbitals

(34) These would include differences in phase matching loci, as realignment of the short Ti=O bonds more closely with the polar axis would cause elongation of the major axis at the expense of the minor axes. However, the SHG intensity data reported in this work are derived from crystallites smaller than the expected coherence lengths, and this factor does not come into play.

(35) Burdett, J. K.; Hughbanks, T. *Inorg. Chem.* **1985**, *24*, 1741. Burdett, J. K. *Inorg. Chem.* **1985**, *24*, 2244.
(36) Williams, D. J. *Angew. Chem., Int. Ed. Engl.* **1984**, *23*, 690–703.
(37) Phillips, M. L. F.; Harrison, W. T. A.; Gier, T. E.; Stucky, G. D.; Kulkarni, G. V.; Burdett, J. K. *Inorg. Chem.* **1990**, *29*, 2158.
(38) Blasse, G.; Brixner, L. H. *Mater. Res. Bull.* **1989**, *24*, 1099. Blasse, G.; Dirksen, G. J.; Brixner, L. H.; Ferretti, A.; Thomas, P. A. *Mater. Chem. Phys.* **1991**, *27*, 279.
(39) Jarman, R. H.; Munowitz, M.; Harrison, J. F. *J. Cryst. Growth* **1991**, *109*, 353.
(40) Jarman, R. H.; Grubb, S. G. *Proc. SPIE—Int. Soc. Opt. Eng.* **1988**, *968*, 108.
(41) Phillips, M. L. F.; Harrison, W. T. A.; Stucky, G. D. *Inorg. Chem.* **1990**, *29*, 3245.

to become less oxygen-like, limiting the degree of excited-state mixing possible.[37]

These effects are manifested to a greater degree in the KTP-type structures reported in this work. Upon exchange for Na or Ag, the average cation–oxygen coordination distance drops from 2.9 to 2.6 Å, indicating a generally closer association of the cation with the framework. The differences lie in the relative preferences of the cations for the $(Ti–O)_n$ and the PO_4 (or AsO_4) oxygen atoms. In NaTP, as in KTP, the average bond valences for the Na–O(9,10) and the Na–O(1–8) interactions are essentially the same, so the optical nonlinearity of NaTP is impacted only by the overall closer sodium–oxygen contacts. In AgTP, silver plainly favors coordination with the titanyl oxygen atom O(9), disrupting conjugation in the $(Ti–O)_n$ chain. In NaTA, the closer coordination of sodium to the framework is counteracted by the increased basicity of the AsO_4 groups, which in effect draw these ions away from the titanyl chain. In this respect, NaTA behaves more like KTA than NaTP.

The low SHG intensity of AgTP is thus readily explained by both the high electronegativity of Ag (relative to K) and the strong coordination of Ag(1) and Ag(2) to the titanyl oxygen atoms. Similarly, the close association of Na with the Ti–O framework oxygen atoms reduces SHG intensity by an order of magnitude despite the similar electronegativities of Na and K. The looser Na coordination with the titanyl oxygen atoms in NaTA allows this material to have a strong nonlinear response. In addition, the effects of any increase in cation–framework covalency are likely to be mitigated by arsenate substitution, which should increase the basicity of the oxygen levels, facilitating their mixing with the metallic charge-transfer band orbitals.

6. Summary

For small cation isovalent analogues of KTP (e.g., α-$NaTiOPO_4$, α-$AgTiOPO_4$, and α-$NaTiOAsO_4$) the titanite ($CaTiOSiO_4$) structure is found to be thermodynamically favored at high temperature. Through ion exchange, however, we have synthesized β-$NaTiOPO_4$, β-$AgTiOPO_4$, and β-$NaTiOAsO_4$, three KTP isostructures which cannot be prepared directly from their constituent oxides. Though their Ti coordination environments are similar to those in KTP and KTA, their SHG intensities vary over 2 orders of magnitude. The Na and Ag atoms in these structures are lower coordinate than are the K atoms in KTP, probably due to their reduced size. Because NaTP and AgTP retain the long–short Ti–O bonding characteristic of KTP and other ferroelectric metal oxides with good NLO properties, localized bond-charge models do not adequately predict the low SHG intensities observed in these compounds. However, the correlation between SHG intensity and cation coordination and electronegativity agrees with the predictions of a more extended model in which cation–Ti–O(9,10) interactions alter excited-state mixing coefficients for a charge-transfer state and thereby influence nonlinear susceptibility. This is confirmed by single-crystal structural data and nonlinear optical results previously reported for KTP and KTA.

Acknowledgment. This work was supported by the United States Department of Energy under Contract DE-AC04-76DP00789 (M.L.F.P.). Additional support was provided by the National Science Foundation (DMR) (G.D.S.) and E. I. du Pont de Nemours (E.M.M.).

Registry No. $Ag_{0.5}K_{0.5}TiOPO_4$, 138312-50-2; $Ag_{0.85}K_{0.15}TiOPO_4$, 124520-05-4; $Na_{0.2}K_{0.8}TiOPO_4$, 127005-70-3; $Na_{0.4}K_{0.6}TiOPO_4$, 127005-72-5; $Na_{0.55}K_{0.45}TiOPO_4$, 138312-51-3; $Na_{0.65}K_{0.35}TiOPO_4$, 138312-52-4; $Na_{0.95}K_{0.05}TiOPO_4$, 138312-53-5; $K_{0.13}Na_{0.87}TiOASO_4$, 138312-54-6; $NaTiOPO_4$, 110074-73-2.

Supplementary Material Available: Tables of anisotropic thermal parameters and all bond distances and angles within 3.2 Å (9 pages); tables of calculated and observed structure factors (24 pages). Ordering information is given on any current masthead page.

Effect of Silica on the Nonoxidative Thermal Degradation of Poly(vinyl butyral)

Robert L. White* and Jiu Ai

Department of Chemistry and Biochemistry, University of Oklahoma, Norman, Oklahoma 73019

Received September 17, 1991. Revised Manuscript Received November 19, 1991

Thermal degradation processes for poly(vinyl butyral) (PVB) are examined over the temperature range 50–1000 °C. The thermal degradation of neat PVB, PVB coated on silica, and PVB coated on silanized silica are compared. Thermal degradation of PVB in contact with silica proceeds through four stages. At low temperature, water is generated due to dehydroxylation. A second stage occurs between 350 and 450 °C, corresponds to the largest sample mass loss, and is characterized by evolution of oxygen-containing species. The third stage occurs between 400 and 600 °C and is characterized by evolution of unsaturated and aromatic species. The last degradation stage occurs between 600 and 800 °C and corresponds to removal of carbon-rich residue by the water–gas reaction. The water–gas reaction is inhibited by the presence of H_2.

Introduction

The increasing size and complexity of new integrated circuit (IC) designs has created a need for high-quality IC packaging technology. Substrate materials employed in IC packaging should be impermeable to moisture and have high resistance, high thermal conductivity, and a coefficient of thermal expansion that closely matches that for silicon. Ceramics possess these characteristics and are the materials of choice for constructing high-performance integrated circuit packages.[1]

Polymers are used in the ceramics industry as binders

(1) Aldinger, F. In *High-Tech Ceramics*; Kostorz, G., Ed.; Academic Press: New York, 1989; pp 161–179.

0897-4756/92/2804-0233$03.00/0